Author's Accepted Manuscript

Productivity analysis for a vertically fractured well under non-Darcy flow condition

Wanjing Luo, Xiaodong Wang, Yin Feng, Changfu Tang, Yingfang Zhou

Cite this article as: Wanjing Luo, Xiaodong Wang, Yin Feng, Changfu Tang and Yingfang Zhou, Productivity analysis for a vertically fractured well under non-Darcy flow condition, *Journal of Petroleum Science and Engineering,* http://dx.doi.org/10.1016/j.petrol.2016.07.003

Productivity analysis for a vertically fractured well

under non-Darcy flow condition

Wanjing Luo [a]*, Xiaodong Wang [a] , Yin Feng[b]，Changfu Tang[c]，Yingfang Zhou[d]

a. School of Energy Resources, China University of Geosciences (Beijing), Beijing, China, 100083

b. University of Louisiana at Lafayette, Lafayette, LA, USA 70504

c. Exploration Research Institute, Anhui Provincial Bureau of Coal Geology, Hefei, Anhui 230088

d. School of engineering, university of Aberdeen, Aberdeen, the UK AB24 3DB

* Corresponding author: luowanjing@cugb.edu.cn

Abstract

In this paper, a semi-analytical solution of the pseudosteady-state (PSS) productivity index under non-Darcy flow condition is proposed. Based on the model, a new method of optimization of the fracture conductivity has been developed for non-Darcy flow in the fracture. Meanwhile, the effects of the Reynolds number, the proppant number and the fracture conductivity on the dimensionless productivity index have been discussed in detail.

Results show that: (1) the classic UFD (Unified Fracture Design) curves of the Darcy-flow model underestimate the effect of the proppant number and are unsuitable for the non-Darcy-flow fracture optimization. Our discretized model provides a new tool to obtain the optimal fracture parameters for the case of non-Darcy flow condition. (2) for a given penetration ratio, the non-Darcy flow behavior exerts a strong influence on the productivity index with the dimensionless fracture conductivity C_{fD}= 0.1 -1000 and a considerable productivity index drop can be observed. For the extremely low (C_{fD}<0.1) or high (C_{fD}>1000) dimensionless fracture conductivity, the effect of non-Darcy flow becomes negligible. (3) the effect of the non-Darcy flow on the productivity index becomes pronounced at large value

of proppant number, N_p. For a given proppant number, the optimal fracture conductivity is slowly increasing as the Reynolds number increases. However, the magnitude of the effect on the productivity index is gradually declining. At the Reynolds number less than 5, the non-Darcy flow has a relatively strong impact on the productivity index and an apparent fall of the maximum productivity index can be noticed, especially for a large proppant number. Beyond the value of 5, the declining trend of the maximum productivity index gradually slows down as the Reynolds number increases.

Kewords: productivity index; non-Darcy flow; vertically fractured well; optimization of the fracture parameters; rectangular reservoir

Introduction

As an efficient stimulation technique, hydraulic fracturing has been widely used to increase productivity index (PI) by increasing production rate or decreasing pressure drawdown, especially for tight / shale oil/ gas reservoirs.

Mathematical models have been widely used to calculate the productivity of a fractured well under Darcy flow condition. Prats (1961) introduced the concept of equivalent wellbore radius to consider the effect of the fracture. Reymond and Blinder (1967) provided ways of designing fracture treatments and evaluating their results in a damaged formation with a mathematical model relating stimulation ratio

to the relative conductivity of fractures. They showed that their model was in agreement with the McGuire-Sikora curves for the fracture penetration ratios less than one-half of the drainage radius. The effects of fracture penetration ratio on reciprocal effective wellbore radius have been presented for the uniform-flux and infinite-conductivity fracture (Gringarten and Ramey, 1974; Raghvan et al., 1978). Cinco-Ley and Samaniego (1981) introduced a pseudo-skin function to characterize the impact of a finite-conductivity fracture on the performance of a vertical well. Riley et al. (1991) provided a solution for the equivalent wellbore radius based on the assumption of elliptical finite-conductivity fractures. According to the definition of pseudo-skin and pseudo-skin function, dimensionless pseudo-steady state (PSS) productivity index can be expressed by three parameters, i.e., boundary radius, half length of a fracture and pseudo-skin function. In calculations, it was convenient to use an explicit expression to replace the pseudo-skin function (Economides et al., 2002).

ValkÓ and Economides (1998) introduced the concept of proppant number and proposed the UFD (Unified Fracture Design) method for conductivity optimization. For a fixed proppant number, the maximum productivity index can be achieved by fracture conductivity optimization in a square drainage area. Diego J.Romero et al. (2003) extended ValkÓ-Economides method to a stimulated well with fracture faces and choke skins. A.S. Demarchos et al. (2004) pushed the physical limits of fracturing in a wide range of reservoirs with a series of parametric studies. Meyer and Jacot (2005) used the pseudosteady-state resistivity model to calculate the

3

productivity of a fractured well. Daal and Economides (2006) calculated the pseudosteady-state productivity index of a fractured well in a rectangular drainage area using the Direct Boundary method. Wang and Jia (2014) established a model to calculate the productivity of multi-fractured horizontal well.

For a fractured gas well, the effect of non-Darcy flow on the productivity cannot be ignored (Holditch and Morse, 1976; Guppy et al., 1982a, b). Vincent et al. (1999) presented several cases of non-Darcy flow effects on productivity. For a specified mass of proppant, a shorter and wider fracture can be used to compensate for the non-Darcy effects (Vincent et al., 1999 ; Hernandez, 2004 ; Kakar et al., 2004). Gil et al. (2003) discussed the design and analysis of fractured-gas-well tests for the case of non-Darcy flow within the fracture. They used a rate-dependent skin to represent the additional pressure drop caused by the effect of non-Darcy flow. They pointed out that non-Darcy flow effect may be reduced to tolerate ranges by design considerations. An effective permeability was introduced to account for the effect of non-Darcy flow (Henry D. Lopez-Hernandez et al., 2004; Y. Wei and Economides, 2005). Based on the definition of the effective permeability, the equation form of non-Darcy flow can be transformed into Darcy flow equation form. Thus the *ValkÓ-Economides* optimization curves (UFD curves) and an iterative process started with a Reynolds number guess have been used to obtain the maximum productivity index and optimal fracture conductivity. Zeng and Zhao (2010) also presented a different optimal method for a vertical fractured well under non-Darcy flow effects. Based on the assumption of the infinite homogeneous

4

reservoir, a constant value of 0.5 with the pressure derivatives was chosen as the pseudo-steady state characteristic for hydraulically fractured wells. They suggested that the fracture geometry optimization could involve two stages: fracture volume optimization and fracture length optimization.

As can be seen from the literature review above, the fracture can be handled by three methods for the productivity calculation. Firstly, the finite-conductivity fracture can be taken as an equivalent parameter, for example, equivalent wellbore radius (Prats, 1961; Gringarten and Ramey, 1974; Raghvan et al., 1978; Riley et al., 1991), pseudo-skin function (Cinco-Ley and Samaniego, 1981; Economides et al., 2002). This method is relatively simple and easy to calculate. However, it is difficult to extend. Secondly, the fracture can be approximately replaced by multi-equally spaced point-source wells (Direct Boundary method) (ValkÓ and Economides, 1998; Diego J.Romero et al., 2003; A.S. Demarchos et al., 2004; Daal and Economides, 2006). Without the fracture flow model, it is hard to incorporate non-Darcy flow effects. Thus, an effective permeability model has been introduced to transform non-Darcy flow model into the Darcy flow model (Henry D. Lopez-Hernandez et al., 2004; Y. Wei and Economides, 2005). Lastly, the fracture has been divided into *n* segments and each segment can be taken as a short fracture with uniform flow rate. This is a general fracture model which can be used for the Darcy and non-Darcy flow. However, the existing methods for the productivity calculation are based on the assumption of infinite-acting reservoir (Cinco-Ley and Samaniego, 1981; Gil et al., 2003; Zeng and Zhao, 2010).

5

In this paper, a fracture model incorporating into the effect of non-Darcy flow in a rectangular drainage area has been presented. Based on the model, we discussed the effect of the Reynolds number, the fracture conductivity and the proppant number on the productivity index with 2-D and 3-D figures in detail. Then, a new procedure has been employed to obtain the optimal conductivity, maximum productivity index, fracture length and width under non-Darcy flow condition. This method is different from the effective permeability model (Henry D. Lopez-Hernandez et al., 2004; Y.Wei and Economides, 2005) and pseudosteady-state equivalent model (Zeng and Zhao, 2010). This paper is organized as follows : First of all, we present a PSS mathematical model of fluid flow in a fracture in a rectangular drainage area. Secondly, the effects of the parameters on the productivity index are discussed in detail. Then, an application of the optimization is presented to illustrate the advantage of the new model. Finally, some conclusions are made.

2 Mathematical models

2.1 Model descriptions

Fig.1 shows the conceptual model used in this paper. The following assumptions are made.

(1) A vertical well is intercepted by a symmetric fracture with a half length, x_f, in a closed rectangular drainage area. And the fracture is assumed to fully penetrate the reservoir.

(2) The reservoir is of uniform thickness h, porosity φ, and permeability k. A single phase flow in the reservoir is assumed to obey Darcy's law and the viscosity of the fluid is μ. The total compressibility factor, c_t is also uniform.

(3) One-dimensional non-Darcy flow occurs in the fracture. The fracture permeability $k_f(x)$ and width $w_f(x)$ are changing along the fracture. The fracture storage capacity is ignored. The vertically fractured well produces at a constant rate q (oil well) or q_{gsc} (gas well) in the wellbore.

2.2 Dimensionless definitions of the variables

For the sake of simplicity, the following dimensionless variables will be used.

For an oil well, the dimensionless reservoir and fracture pressure are

$$p_D = \frac{2\pi kh(p_i - p)}{q\mu B}, \quad \bar{p}_D = \frac{2\pi kh(p_i - \bar{p})}{q\mu B}, \quad p_{fD} = \frac{2\pi kh(p_i - p_f)}{q\mu B} \tag{1}$$

For a gas well, the dimensionless reservoir and fracture pressure are

$$p_D = \frac{\pi k_g h z_{gsc} T_{gsc}}{p_{gsc} T \mu_g z} \frac{p_i^2 - p^2}{q_{gsc}}, \bar{p}_D = \frac{\pi k_g h z_{gsc} T_{gsc}}{p_{gsc} T \mu_g z} \frac{p_i^2 - \bar{p}^2}{q_{gsc}}, p_{fD} = \frac{\pi k_g h z_{gsc} T_{gsc}}{p_{gsc} T \mu_g z} \frac{p_i^2 - p_f^2}{q_{gsc}} \tag{2}$$

For the fracture flow model, the dimensionless fracture conductivity, C_{fD}, is

$$C_{fD} = \frac{k_f(x) w_f(x)}{k x_f} \tag{3}$$

The penetration ratio in the x direction is defined as

$$I_x = \frac{2x_f}{x_e} \tag{4}$$

The proppant number (Daal and Economides, 2006) is

$$N_p = \frac{2k_f}{k} \frac{V_{prop}}{V_{res}} \tag{5}$$

7

From the definition of the penetration ratio and dimensionless fracture conductivity, we obtain

$$N_p = \frac{2k_f}{k}\frac{V_{prop}}{V_{res}} = \frac{4k_f x_f w h}{k x_e y_e h} = C_{fD}I_x^2\frac{x_e}{y_e} \tag{6}$$

The dimensionless flow rate of the *i*-th segment for the oil well and gas well are given as

$$q_{fDi} = \frac{\tilde{q}_f L_{fi}}{q}, \quad q_{gscfDi} = \frac{\tilde{q}_f L_{fi}}{q_{gsc}} \tag{7}$$

For an oil well, the dimensionless productivity index in the wellbore is

$$J_D = \frac{q}{\bar{p} - p_w}\frac{B\mu}{2\pi kh} \tag{8}$$

For a gas well, the dimensionless productivity index in the wellbore is

$$J_D = \frac{q_{gsc}}{\bar{p}^2 - p_w^2}\frac{p_{gsc}T\mu_g z}{\pi k_g h z_{gsc}T_{gsc}} \tag{9}$$

Other dimensionless definitions in the reservoir model are

$$L_{fDi} = \frac{L_{fi}}{x_f}; y_D = \frac{y}{x_f}, \quad y_{wD} = \frac{y_w}{x_f}, \quad y_{eD} = \frac{y_e}{x_f}; x_D = \frac{x}{x_f}, x_{wD} = \frac{x_w}{x_f}, x_{eD} = \frac{x_e}{x_f} \tag{10}$$

As can be seen from the dimensionless definitions above, the same dimensionless variables can be obtained by different combinations of the variables for the oil well and gas well. For simplification, we develop the mathematical models for the oil reservoir in Section 2 and Section 3. An example is presented to illustrate the application for a gas well in Section 4.

2.3 Fluid flow in the reservoir

The dimensionless pressure drop of a point located at (x_{Di}, y_{Di}) caused by a

8

point source (x_{wDj}, y_{wDj}) in a rectangular reservoir is presented by Ozkan (1988).

$$p_{Dvi} = \bar{p}_D + 2\pi \frac{y_{eD}}{x_{eD}} \left(\frac{1}{3} - \frac{y_{Di}}{y_{eD}} + \frac{y_{Di}^2 + y_{wDj}^2}{2y_{eD}^2} \right) +$$

$$2\sum_{k=1}^{\infty} \frac{1}{k} \cos k\pi \frac{x_{Di}}{x_{eD}} \cos k\pi \frac{x_{wDj}}{x_{eD}} \frac{chk\pi \left(\dfrac{y_{eD} - |y_{Di} - y_{wDj}|}{x_{eD}} \right) + chk\pi \left(\dfrac{y_{eD} - |y_{Di} + y_{wDj}|}{x_{eD}} \right)}{\left(shk\pi \dfrac{y_{eD}}{x_{eD}} \right)}$$

(11)

The dimensionless pressure drop of a point (x_{Di}, y_{Di}) caused by a segment centered at (x_{wDj}, y_{wDj}) with half length L_{fDi} in the x direction can be obtained by integrating Eq. 11 from x_{wDj} -L_{fDj} to x_{wDj} +L_{fDj} with respect to x_{wDj}.

$$\begin{aligned}
p_{Di} &= \frac{1}{2L_{fDj}} \int_{x_{wDj}-L_{fDj}}^{x_{wDj}+L_{fDj}} p_{Dvi}\left(x_{Di}, y_{Di}, u, y_{wDj}, L_{fDj}, x_{eD}, y_{eD}\right) du \\
&= \bar{p}_D + 2\pi \cdot \left(\frac{y_{eD}}{x_{eD}} \right) \cdot \left(\frac{1}{3} - \frac{y_{Di}}{y_{eD}} + \frac{y_{Di}^2 + y_{wDj}^2}{2y_{eD}^2} \right) \\
&\quad + \left(\frac{2x_{eD}}{\pi L_{fDj}} \right) \sum_{m=1}^{\infty} \left(\frac{F_m}{m^2} \right) \sin\left(\frac{m\pi L_{fDj}}{x_{eD}} \right) \cos\left(\frac{m\pi x_{Di}}{x_{eD}} \right) \cos\left(\frac{m\pi x_{wDj}}{x_{eD}} \right)
\end{aligned}$$

(12)

where

$$F_m = \frac{\cosh\left[\dfrac{m\pi}{x_{eD}}\left(y_{eD} - |y_{Di} - y_{wDj}| \right) \right] + \cosh\left[\dfrac{m\pi}{x_{eD}}\left(y_{eD} - |y_{Di} + y_{wDj}| \right) \right]}{\sinh\left(m\pi \dfrac{y_{eD}}{x_{eD}} \right)}$$

(13)

We define F_{ij} as the influence function

$$F_{ij} = p_{Di} - \bar{p}_D$$

(14)

In fact, The fracture can be divided into $2N$ segments and each segment is taken as a symmetrical fracture located at (x_{wDj}, y_{wDj}) with half length L_{fDj} in the x direction (Fig.2). Regarding the assumption of symmetric fracture, only half of the fracture is considered in the following section. According to the superposition principle, the

9

pressure solution of the point (x_{Di}, y_{Di}) caused by the production of the fracture (2N segments) can be expressed as

$$p_{Di} - \bar{p}_D = \sum_{j=1}^{2N} q_{fDj} \cdot F_{ij}\left(x_{Di}, y_{Di}, x_{wDj}, y_{wDj}, L_{fDj}, x_{eD}, y_{eD}\right), \text{ i=1, 2...N} \tag{15}$$

The sensibility of the discretized segments, 2N, is tested by increasing the number of the segments and comparing the error of the contiguous segment number for different dimensionless fracture conductivity. It is found that the error is decreasing with the increase of discretized segments. We choose the discretized segments, 2N, corresponding to the value of the error less than 1% as the optimal segments. Thus, N=100 and 800 are used for C_{fD} greater than 1 and less than 0.1, respectively. N=400 is used for the calculation while C_{fD} is between 0.1 and 1.

2.4 Fluid flow in the fracture

Luo and Tang (2015) derived a general solution for the varying conductivity fracture under non-Darcy flow condition. In this paper, we present the derivation in brief.

To account for the high velocity flow in the fracture, the following Forchheimer equation will be used (Guppy et al. 1982),

$$\frac{\partial p_f}{\partial x} = \frac{\mu}{k_f(x)}v + \beta\rho v^2 \tag{16}$$

where v is flow velocity in the fracture, ρ is fluid density, and the term β is called the "β factor" (Guppy et al.,1982). Eq.16 can be written in the form of Darcy flow

$$\left(\frac{k_{f,app}(x)}{\mu}\right) \cdot \left(\frac{\partial p_f}{\partial x}\right) = \left(\frac{q_c B}{w_f(x)h}\right) \tag{17}$$

The apparent fracture permeability in Eq. 17 is defined as

$$k_{f,app}(x) = \frac{k_f(x)}{1 + \beta k_f(x)\rho v / \mu} \tag{18}$$

In order to analyze the effect of non-Darcy flow in the fracture, the Reynolds number was defined as

$$N_{\mathrm{Re}} = \frac{k_f \beta \rho}{w_f h \mu} \cdot q \tag{19}$$

Substituting Eq.19 into Eq.18 yields

$$k_{f,app}(x) = k_f(x)\frac{1}{1 + N_{\mathrm{Re}}q_{cD}} \tag{20}$$

Thus, Eq.17 can be written in the following dimensionless form

$$\frac{C_{fD}(x_D)}{1 + N_{\mathrm{Re}} \cdot q_{cD}}\left(\frac{\partial p_{fD}}{\partial x_D}\right) + 2\pi\, q_{cD} = 0 \tag{21}$$

Combination of the inner and outer boundary conditions results in the discretized form of the fracture model (Luo and Tang, 2015)

$$p_{wD} - p_{fDi} = \left(\frac{2\pi}{\hat{C}_{fD}}\right) \cdot \left[\begin{array}{l} \xi_{Di} \cdot \sum_{j=1}^{N} q_{fDj} - \dfrac{(\xi_{Di} - \xi_{Di-1/2})^2}{2 \cdot \Delta\xi_{Di}} \cdot q_{fDi} \\ - \sum_{j=1}^{i-1}\left(\dfrac{\Delta\xi_{Dj}}{2} + \xi_{Di} - \sum_{n=1}^{j}\Delta\xi_{Dn}\right) \cdot q_{fDj} \end{array}\right] \tag{22}$$

where

$$\xi_D = \xi_D(x_D) = \hat{C}_{fD} \cdot \int_0^{x_D}\frac{dx_D}{C_{fD}(x_D)} \tag{23}$$

$$\hat{C}_{fD} = 1/\int_0^1\frac{dx_D}{C_{fD}(x_D)}, \quad x_D \in [0,1] \tag{24}$$

11

2.5 Productivity index of a fractured well

The dimensionless productivity index of the *i*-th segment can be defined as

$$J_{Di} = -\frac{q_{fDi}}{\bar{p}_D - p_{wD}} \tag{25}$$

The corresponding total dimensionless productivity index of the oil well in the wellbore is

$$J_D = \left(\frac{B\mu}{2\pi kh}\right) \cdot \left(\frac{q}{\bar{p} - p_w}\right) = -2\frac{\sum_{i=1}^{N} q_{fDi}}{\bar{p}_D - p_{wD}} = 2 \cdot \sum_{i=1}^{N} J_{Di} \tag{26}$$

The PSS equation (Eq.15) and the fracture equation (Eq.22) of the i-th segment can be further expressed as

$$p_{Di} - \bar{p}_D = \sum_{j=1}^{N} q_{fDj} \cdot (F_{ij} + F_{i,j+N}) \tag{27a}$$

$$p_{wD} - p_{fDi} = \sum_{j=1}^{N} q_{fDj} \cdot A_{ij} \tag{27b}$$

According to the continuity condition, for the pressure and the flux to be continuous along the fracture surface, the following conditions must hold along the fracture segment

$$p_{Di}\left(x_{Di}, y_{Di}\right) = p_{fDi}\left(x_{Di}, y_{Di}\right), \quad q_{Di}\left(x_{Di}, y_{Di}\right) = q_{fDi}\left(x_{Di}, y_{Di}\right) \tag{28}$$

Substituting Eq.27b and Eq.28 into Eq.27a yields

$$\bar{p}_D - p_{wD} = -\sum_{j=1}^{N} q_{fDj} \cdot (F_{ij} + F_{i,j+N}) - \sum_{j=1}^{N} q_{fDj} \cdot A_{ij} \ , \quad i=1, 2, \dots, N \tag{29}$$

By substituting Eq.25 into Eq.29, we obtain

$$\sum_{j=1}^{N} J_{Dj} \cdot (F_{ij} + F_{i,j+N} + A_{ij}) = 1 \ , \quad i=1, 2, \dots, N \tag{30}$$

Eq.30 can be written in matrix form as

$$(\vec{F} + \vec{A}) \cdot \vec{J} = 1 \tag{31}$$

Where

$$\vec{J} = \begin{pmatrix} J_{D1} \\ J_{D2} \\ \vdots \\ J_{DN} \end{pmatrix}, \quad \vec{A} = \begin{pmatrix} a_{11} & \cdots & a_{1j} & \cdots & a_{1N} \\ \vdots & \vdots & \vdots & \vdots & \vdots \\ a_{i1} & \cdots & a_{ij} & \cdots & a_{iN} \\ \vdots & \vdots & \vdots & \vdots & \vdots \\ a_{N1} & \cdots & a_{Nj} & \cdots & a_{NN} \end{pmatrix} \tag{32}$$

$$\vec{F} = \begin{pmatrix} F_{11} + F_{1,N+1} & F_{12} + F_{1,N+2} & \cdots & F_{1N} + F_{1,N+N} \\ F_{21} + F_{2,N+1} & F_{22} + F_{2,N+2} & \cdots & F_{2N} + F_{2,N+N} \\ \vdots & \vdots & \ddots & \vdots \\ F_{N1} + F_{N,N+1} & F_{N2} + F_{N,N+2} & \cdots & F_{NN} + F_{N,N+N} \end{pmatrix} \tag{33}$$

The calculation of a_{ij} is presented by Luo and Tang (2015) in detail.

By solving Eq.31, the dimensionless productivity index J_{Di} of each segment can be obtained. Then the total productivity index J_D of the vertical fracture in the wellbore can be calculated by Eq.25.

3 Results

3.1 Verification of the model

We compare our solutions with results presented by ValkÓ and Economides (1998). As shown in Table 1, our results are highly consistent with the results when the dimensionless fracture conductivity is greater than 1. For the case of the low dimensionless fracture conductivity, the variance can be observed which is caused by the discretized segments, different calculation methods and selection of the pressure point for calculation. ValkÓ and Economides introduced many point sources (vertical wells) to approximately represent the fracture and the calculated pressure point is at (x_{wD}, $y_{wD}+ \varepsilon$) for the point source instead of a line source (fracture)

13

calculated at (x_{wD}, y_{wD}) in this paper.

3.2 Effect of the fracture penetration ratio and Reynolds number on the productivity index

Fig.3 illustrates the effect of the fracture penetration ratio (I_x) and Reynolds number (N_{Re}) on the dimensionless productivity index (J_D) in a square drainage area. It is shown that J_D increases as the penetration ratio increases at the same fracture conductivity. For a specific penetration ratio, there is a slight rise of J_D when C_{fD} is below 0.1. In the range of 0.1 to 1000 for C_{fD}, a relatively rapid increase of J_D can be observed, especially for the high penetration ratio ($I_x=0.8$). The curves flatten out at large C_{fD} which delineates the infinite-conductivity fracture performance. Moreover, the existence of non-Darcy flow ($N_{Re}>0$) in the fracture will result in the reduction of J_D compared with the Darcy flow ($N_{Re}=0$, black line). A stronger effect can be found when the fracture conductivity, C_{fD}, is in the range of 0.1-1000 with a large penetration ratio ($I_x=0. 8$).

3.3 Dimensionless productivity index J_D at N_p less than 0.1

The effects of the Reynolds number, the fracture conductivity and the proppant number on the productivity index are presented in Fig.4 through Fig.12 for the case of low proppant number ($N_p<0.1$). Some 2-D and 3-D figures are used to elaborate the effects.

Fig.4 shows the dimensionless productivity index as a function of

dimensionless fracture conductivity with the proppant number as a parameter for N_p<0.1 under the Darcy flow condition. This figure was first drawn by ValkÓ and Economides (1998), who pointed out that for a given value of N_p, the maximum productivity index is achieved at a well-defined value of the dimensionless fracture conductivity located at the peak of the individual curve. At proppant numbers less than 0.1, the dimensionless fracture conductivity corresponding to the maximum J_D will always occur at C_{fD}=1.6.

For non-Darcy flow in the fracture, the Reynolds number exerts great influence on the dimensionless productivity index. As shown in Fig.5, the optimal conductivities will not stay constant at C_{fD}=1.6 but fluctuate around C_{fD}=3.06 for the case of N_{Re}=10.

Fig.6 further reveals the effect of the Reynolds number on the productivity index at a proppant number of 0.01. With the increase of the Reynolds number, the optimal conductivity becomes larger and a steady fall in the productivity index can be noticed. The optimal conductivity is at C_{fD}=1.6 corresponding to the Darcy flow while it is 4.296 at the Reynolds number equal to 20. Meanwhile, the maximum productivity index reduces from 0.304 at N_{Re}=0 to 0.263 at N_{Re}=20.

In addition, some 3-D color figures and their top views are presented to illustrate the effects of both the fracture conductivity and the Reynolds number on the productivity index for a given proppant number in Fig.7 through Fig.12. For an extremely low proppant number, such as N_p=0.0003, the Reynolds number has a relatively weak impact on the productivity index. The peak of the J_D curve (Fig.7)

drops steadily with the increase of the Reynolds number. The optimal fracture conductivity changes from 1.6 at N_{Re}=0 to 3.2 at N_{Re} =20 (Fig.8). On the contrary, for a relatively large proppant number, such as N_p=0.03, a considerable fall of the peak of the J_D curve (Fig.11) can be noticed at a low Reynolds number. The scope of the optimal fracture conductivity is between 1.6 and 4.47 (Fig.12).

In general, the effect of non-Darcy flow on the productivity index becomes more and more significant with the increase of the proppant number. However, the magnitude of the effect is gradually declining as the Reynolds number increases for a given proppant number (Fig.7, Fig.9 and Fig.11). Comparing with Fig.8, Fig.10 and Fig.12, an approximate linear relationship on a semi-log plot between the Reynolds number and the optimal fracture conductivity corresponding to the maximum productivity index can be observed when the Reynolds number is greater than 5. Moreover, the relatively stronger impact on the productivity index occurs at Reynolds number less than 5 (Fig.7 through Fig.12).

3.4 Dimensionless productivity index J_D at N_p greater than 0.1

Fig.13 and Fig.14 present the J_D curves with the Darcy and non-Darcy flow effect at N_p greater than 0.1, respectively. The maximum productivity index increases with increase in the proppant number. The effect of the non- Darcy flow will not change the trend of the curves, but decrease the range of the optimal conductivity C_{fD} from 1.96-100 at N_{Re}=0 to 4.7-100 at N_{Re} =10. Comparing Fig.6 with Fig.15, the same phenomena can be found that the presence of non-Darcy flow

16

reduces the productivity index and enlarges the optimal fracture conductivity. However, the effect of the non- Darcy flow at a large proppant number is more obvious than that at a low proppant number. Compared to the Darcy flow in the fracture, the maximum productivity index J_D at N_{Re} =20 drops by 13.5% when N_p= 0.01 (Fig.6) and by 42.89% when N_p= 3 (Fig.15), respectively. In addition, for the infinite-conductivity fracture (C_{fD}>300), the curves with different Reynolds number overlay each other, implying a negligible non-Darcy effect for an extremely large fracture conductivity (Fig.6 and Fig.15).

The 3-D color figures and their top views are presented in Fig.16 through Fig.21 at N_p=0.3, 3, and 30, respectively. For comparison, we use the same scales with C_{fD}=0.1-1000, N_{Re}=0-20 and J_D=0.2-2 to illustrate the curves of the productivity index. As seen, the maximum productivity index drops dramatically when N_{Re} <5 for a large proppant number, such as N_p=3 (Fig.18) and N_p=30 (Fig.20). Beyond the value of 5 for the Reynolds number, the declination of the maximum productivity index gradually slows down (Fig.16, Fig.18 and Fig.20) and an approximate linear relationship on the semi-log plot between the maximum productivity and the fracture conductivity can also be observed just like the cases with the low proppant number (N_p<0.1) (Fig.8, Fig.10, Fig.12, Fig.17, Fig.19 and Fig.21).

3.5 Comparison of our method with the equivalent model

The curves of the productivity index can be used to determinate the optimal

fracture length and width for a given proppant number (ValkÓ and Economides, 1998; Economides et al., 2002; Diego J.Romero et al., 2003; Daal and Economides, 2006). The UFD (Unified Fracture Design) method has been widely used for the fracture design under the Darcy flow condition (Economides et al., 2002). For non-Darcy flow in the fracture, an approximately equivalent model which introduces the concept of the effective permeability to transform non-Darcy flow into Darcy flow was developed to obtain the optimal fracture length and width by using the Darcy-flow curves of the productivity index (Henry D. Lopez-Hernandez et al., 2004; Y. Wei and Economides, 2005). In this section, we discuss the adaptability of the equivalent model to deal with non-Darcy flow in the fracture.

The parameters of a circular drainage area presented by Henry D. Lopez-Hernandez et al. (2004) were used to calculate the productivity index (Table 2). Although our model is based on the assumption of the rectangular drainage area, it can also be used to calculate the performance of the circular drainage area when $x_e = y_e = \sqrt{\pi} r_e$ (Ozkan, 1988; Economides et al., 2002).

We calculate the proppant number.

Reservoir volume (V_{res})

$$V_{res} = \pi r_e^2 h = \pi \times 745^2 \times 39 = 6.8 \times 10^7 \ ft^3 \tag{34}$$

The volume of proppant injected (V_{i-2w})

$$V_{i-2w} = \frac{0.016(M_{p-2w})}{(1-\phi_p)SG_P} = \frac{0.016 \times (60,000)}{(1-0.40) \times 2.62} = 610 \ ft^3 \tag{35}$$

Volume of proppant reaching the pay (V_{p-2w}) is estimated from the ratio of pay to the fracture height:

$$V_{p\text{-}2w} = V_{i\text{-}2w} \frac{h}{h_f} = 610 \times \frac{39}{139} = 171 \ ft^3 \tag{36}$$

The real proppant number (N_p) is obtained from

$$N_p = \frac{2k_f}{k_g} \frac{V_{p-2w}}{V_{res}} = \frac{2 \times 134248}{0.2} \frac{171}{6.8 \times 10^7} = 3.383 \tag{37}$$

In the case of non-Darcy flow condition, Henry D. Lopez-Hernandez et al. (2004) introduced the concept of the effective permeability to calculate the proppant number. We name it as an equivalent proppant number in this paper.

For a Reynolds number guess, such as $N_{Re}=9.82$, the effective permeability

$$k_{f-eff} = \frac{k_f}{1 + N_{Re}} = \frac{134248}{1 + 9.82} = 12407 \ md \tag{38}$$

And the equivalent proppant number

$$N_p = \frac{2k_{f-eff}}{k_g} \frac{V_{p-2w}}{V_{res}} = \frac{2 \times 12407}{0.2} \frac{171}{6.8 \times 10^7} = 0.31 \tag{39}$$

The Darcy-flow curve of the productivity index at $N_{Re}=0$ and $N_p=0.31$ which represents the non-Darcy-flow curve at $N_{Re}=9.82$ and $N_p=3.383$ was used to obtain the maximum productivity index (Henry D. Lopez-Hernandez et al., 2004).

In order to reveal the difference between the two methods, the equivalent proppant number under different Reynolds number is calculated (Table 3).

Fig.22 illustrates the comparison of our model (red lines) with Henry D. Lopez-Hernandez et al. method (black lines). The dots and the blue lines denote the maximum productivity index on each curve. It is shown that a huge difference can be observed and the difference becomes larger as the Reynolds number increases (blue lines). The errors of the optimal fracture conductivity of the two methods are

between 49.14% and 80.43%, while it is from 15.75% to 29.66% of the errors of the maximum productivity index when N_{Re}=2 to 20 (Table 3).

As discussed, the equivalent model (Henry D. Lopez-Hernandez et al., 2004; Y. Wei and Economides, 2005) which underestimates the effect of the proppant number will lead to a large error for calculation of the maximum productivity index and optimal fracture conductivity. Thus, it is not suitable for fracture optimization under non-Darcy flow condition.

4 Application

Based on the non-Darcy-flow model developed in this study, a method to determine the optimal fracture parameters is proposed. As stated by Henry D. Lopez-Hernandez et al. (2004), an iterative process starts with a Reynolds number guess. A new Reynolds number is calculated at the end of the process. The iteration stops when error in step 6 is 0.1% or less. For comparison, the parameters presented by Henry D. Lopez-Hernandez et al. (2004) are used (Table 2).

(1) Calculate optimal dimensionless fracture conductivity (C_{fDopt}) and optimal dimensionless productivity index (J_{Dopt})

By setting an initial guess of the Reynolds number as 16.5, the curve of the productivity index with N_p=3.383 and N_{Re}=16.5 is presented in Fig.23. As can be seen, the maximum productivity index is 0.7655 corresponding to the dimensionless fracture conductivity 9.942, i.e, $C_{fDopt} = 9.942$ and $J_{Dopt} = 0.7655$.

(2) Calculate optimal fracture dimensions

Optimal fracture length (x_f)

$$x_f = \left(\frac{k_f V_{p-1w}}{C_{fDopt} k_g h} \right)^{\frac{1}{2}} = \left(\frac{134248 \times 85.5}{9.942 \times 0.2 \times 39} \right)^{\frac{1}{2}} = 385.113 \qquad (40)$$

The optimal propped width (w_f)

$$w_f = \left(\frac{C_{fDopt} k_g V_{p-1w}}{k_f h} \right)^{\frac{1}{2}} = \left(\frac{9.942 \times 0.2 \times 85.5}{134248 \times 39} \right)^{\frac{1}{2}} = 0.00570 \qquad (41)$$

(3) Calculate gas production (q_{gsc})

$$q_{gsc} = \frac{k_g h(p_{res}^2 - p_w^2)}{1,424 \mu_g z T_{res}} J_{Dopt} \qquad Mscf / day \qquad (42)$$
$$= \frac{0.2 \times 39 \times (5254^2 - 1400^2)}{1424 \times 0.0205 \times 0.944 \times 680} \times 0.7655 = 8171.27$$

(4) Calculate gas velocity within the fracture

Gas formation volume factor (B_g)

$$B_g = 0.0282 \frac{z T_{res}}{p_w} = 0.0282 \times \frac{0.934 \times 680}{1400} = 0.0129 \quad \frac{rcf}{scf} \qquad (43)$$

Gas velocity (v)

$$v = \frac{500 B_g q_{gsc}}{h_f w_f} = \frac{500 \times 0.0129 \times 8171.27}{139 \times 0.00570} = 66628.773 \quad ft / day \qquad (44)$$

(5) Calculate the Reynolds number

Molecular weight of the mixture (M_g)

$$M_g = M_{air} \cdot SG_g = 29 \times 0.644 = 18.68 \qquad (45)$$

Density of the gas (ρ_g)

$$\rho_g = \frac{p_w M_g}{z R T_{res}} \qquad (46)$$

$$R = 10.732 \quad \frac{psia \cdot ft^3}{lb \cdot mole \cdot ^\circ R} \qquad (47)$$

z-factor is calculated at wellbore flowing conditions.

21

Therefore,

$$\rho_g = \frac{1400 \times 18.68}{0.934 \times 10.732 \times 680} = 3.7953 \quad lbm / ft^3 \tag{48}$$

Beta factor (β)

$$\beta = \frac{a}{k_f^b \phi_p^c} = \frac{3.47 \times 10^{11}}{134248^{1.35} \times 0.40^0} = 41462 \tag{49}$$

Reynolds number (N_{Re})

$$N_{Re} = 1.83 \times 10^{-16} \frac{\beta k_f \rho_g v}{\mu_g}$$

$$= 1.83 \times 10^{-16} \times \frac{41462 \times 134248 \times 3.7953 \times 66628.773}{0.0156} = 16.512 \tag{50}$$

(6) Error of Reynolds number

$$Error = \frac{\left| N_{Re_{new}} - N_{Re_{old}} \right|}{N_{Re_{old}}} \times 100 = \frac{|16.5 - 16.512|}{16.5} \times 100 = 0.073\% \tag{51}$$

By comparing with Henry D. Lopez-Hernandez et al. results, it is shown that a greater productivity index can be achieved with a longer and narrower fracture (Table 4).

5 Conclusions

This paper focuses on the PSS productivity index in a rectangular reservoir. According to the results and observations, some conclusions can be drawn as follows:

(1) Unlike the existing model, a line source has been used to describe the fracture instead of the point source. The characteristic of the fluid flow of the line source is more close to the fluid flow in the fracture than the point source. Based on the line-source model, a semi-analytical solution of the PSS productivity index under

non-Darcy flow condition is proposed.

(2) It is difficult to consider the effect of non-Darcy flow in the fracture for the existing point-source model. Thus, an equivalent model for non-Darcy flow (Henry D. Lopez-Hernandez et al., 2004; Y. Wei and Economides, 2005) has been used to approximately calculate the productivity index. It is shown that the equivalent model underestimates the effect of the proppant number and leads to large errors in calculation of the maximum productivity index. This equivalent model is unsuitable for the optimization for the fracture conductivity under non-Darcy flow condition. A new and accurate method is presented for the fracture optimization accounting for the effect of non-Darcy flow in the fracture.

(3) For a given penetration ratio, the presence of non-Darcy flow in the fracture makes productivity index drop compared with the Darcy flow. For a large penetration ratio, a stronger effect can be found in the range of the fracture conductivity C_{fD} =0.1-1000. The effect of non-Darcy flow can be ignored for extremely large fracture conductivity (C_{fD}>1000).

(4) In general, the presence of non-Darcy flow reduces the productivity index and increases the optimal fracture conductivity for a given proppant number. Moreover, the effect of non-Darcy flow on the productivity index becomes more significant with the increase of the proppant number. However, the magnitude of the effect gradually declines as the Reynolds number increases for a given proppant number.

(5) When the Reynolds number is less than 5, it has a strong impact on the

23

productivity index and an apparent fall in maximum productivity index can be noticed, especially for the large proppant number. Beyond the value of 5, the declining trend of the maximum productivity index gradually slows down. An approximately linear relationship on the semi-log plot between the Reynolds number and the optimal fracture conductivity can be observed when the Reynolds number is greater than 5.

Nomenclature

B Volume factor, RB/STB

C_{fD} dimensionless fracture conductivity

h net pay, ft

h_f fracture height, ft

I_x penetration ratio

J_D dimensionless productivity index

k resrevoirreservoir permeability, md

k_f fracture permeability, md

$k_{f\text{-eff}}$ effective permeability of non-Darcy flow in the fracture, md

L_f half length of a discretization segment

M_{air} molecular weight of air, lb/lb mole

M_g molecular weight of gas mixture, lb/lb mole

$M_{p\text{-}2w}$ injected proppant mass, lbm

N_{Re} Reynolds number

$N_{Re\ new}$ Reynolds number calculated at the end of actual iteration

$N_{Re\ old}$ Reynolds number calculated in the previous iteration

N_p proppant number

p pressure, psi

$\overline{p}$ average pressure, psi

p_i initial formation pressure, psi

p_f fracture pressure, psi

p_{wf} wellbore pressure, psi

q total oil rate in wellbore, STB /day

$\tilde{q}_f$ flow rate of per unit fracture length from formation, i.e., flow rate

strength, STB /d/ft

q_{fDi} dimensionless flow rate of the i-th segment

q_{gsc} gas rate production at standard conditions, Mscf/day

q_{cD} dimensionless cross-sectional flow rate within the fracture

R   universal constant of gas law, psia.ft^3/(lb. mole. $^\circ R$)

r_e drainage radius, ft

r_w wellbore radius, ft

SG_p proppant specific gravity

SG_g gas specific gravity

T   temperature, $^\circ R$

v gas velocity, ft/day

V   volume, ft^3

V_{p-2w} volume of proppant in the net pay, ft^3

V_{p-1w} volume of proppant in the net pay in one wing, ft^3

V_{i-2w} total volume of proppant to be injected, ft^3

w_f width of the fracture, ft

x coordinate in the x direction, ft

x_w dimensionless wellbore coordinate in the x direction

x_e reservoir length, ft

26

x_f fracture half length, ft

y coordinate in the y direction, ft

y_e reservoir width, ft

y_w dimensionless wellbore coordinate in the y direction

z gas compressibility factor

β non-Darcy flow factor, ft^{-1}

ϕ porosity, fraction

ϕ_p proppant porosity, fraction

μ fluid viscosity, cp

ρ fluid density, lbm/cu ft

ξ_D dimensionless coordinate in the ξ direction

$\Delta\xi_{Di}$ dimensionless discretized step of the *i-th* segment in the ξ direction

   Special Subscripts:

D Dimensionless

f fracture property

g gas well

i initial or segment i

opt   Optimal

res   Reservoir

w wellbore property

gsc   standard conditions

v vertical well (point source)

References

A.S. Demarchos et al. 2004. Pushing the Limits in Hydraulic Fracture Design. SPE-86483. SPE International Symposium and Exhibition on Formation Damage Control, 18-20 February, Lafayette, Louisiana

Cinco-Ley, H. and Samaniego-V. 1981. Transient Pressure Analysis: Finite Conductivity Fracture Case versus Damaged Fracture Case. SPE 10179

Daal and Economides. 2006. Optimization of Hydraulically Fractured Wells in Irregularly Shaped Drainage Areas. SPE-98047. SPE International Symposium and Exhibition on Formation Damage Control, 15-17 February, Lafayette, Louisiana, USA

Diego J.Romero et al. 2003. Optimization of the Productivity Index and the Fracture Geometry of a Stimulated Well With Fracture Face and Choke Skins. SPE-81908-PA. 18(1):57-64

Dyes, A. B., Kemp, C. E. and Caudle, B. H. 1958. Effect of Fractures on Sweep-Out Pattern. Trans., AIME (1958) 213, 245.

Economides, M., Oligney, R., and ValkÓ, P. 2002. Unified Fracture Design, Orsa Press, Alvin, Texas.

Gil et al. 2003. Fractured-Well-Test Design and Analysis in the Presence of Non-Darcy Flow. SPE Reservoir Evaluation & Engineering. 6(03):185-196

Gringarten, A. C., Ramey, H. J., and Raghavan, R. 1974. Unsteady-State Pressure Distributions Created by a Well with a Single Infinite- Conductivity Fracture," SPEJ, August 1974, 347-360.

Guppy, K.H., Cinco-Ley, H., Ramey Jr., H. J. and Samaniego-V. F. 1982. Non-Darcy flow in wells with finite-conductivity vertical fractures. Soc. Pet. Eng. J. 22 (5), 681-698

Guppy, K.H., Cinco-Ley, H., Ramey Jr., H. J. 1982. Pressure buildup analysis of fractured wells producing at high flow rates. J. Pet. Tech. 34(11), 2656-2666

Henry D. Lopez-Hernandez et al. 2004. Optimum Fracture Treatment Design Minimizes the Impact of Non-Darcy Flow Effects. SPE-90195. SPE Annual Technical Conference and Exhibition, 26-29 September, Houston,

Hernandez, H. D. J. L. 2004. Optimal Fracture Treatment Design for Dry Gas Wells maximizes Well performance in the Presence of Non-Darcy Flow Effects. Master thesis. Texas A&M University. Texas.

Holditch, S. A., Morse, R. A., 1976. The effects of non-Darcy flow on the behavior of hydraulically fractured gas wells. JPT 28 (10), 1169-1179. SPE-5586-PA.

John M. Tinsley et al. 1969. Vertical Fracture Height--Its Effect on Steady-State Production Increase. SPE 1900, 633-638, May, 1969

Kakar, A. M. Zheng. S., Stewart. G. 2004. Well test analysis of hydraulically fractured gas wells for non-Darcy flow effects. Presented at the SPE Regional Conference in Pakistan, October 8-9.

Luo and Tang. 2015. A Semianalytical Solution of a Vertical Fractured Well With Varying Conductivity Under Non-Darcy-Flow Condition. SPE-178423-PA

McGuire, W. J. and Sikora, V. J. 1960. The Effect of Vertical Fracture on Well Productivity . Trans., AIME (1960)219, 401-403.

Meyer, B. R., Jacot, R. H. 2005. Pseudosteady-state analysis of finite-conductivity vertical fractures. Paper SPE 95941 presented at the 25th Annual Technical Conference and Exhibition. Dallas, Texas, October 9-12.

Ozkan. 1988. Performance of horizontal wells. Ph.D. Dissertation, the University of Tulsa, Tulsa, OK.

Prats, M.1961. Effect of Vertical Fractures on Reservoir Behavior-Incompressible Fluid Case, SPEJ June, 1961, 105-118.

Raghavan, R. and Hadinoto, Nico. 1978. Analysis of Pressure Data for Fracture Wells: The Constant-Pressure Outer Boundary. SPEJ April, 138-149.

Raymond, L. R., and Binder, G. G. 1967. Productivity of Wells in Vertically Fractured, Damaged Formations. JPT, 120-130

Riley, M.F., Brigham, W.E., Horne, R.N. 1991. Analytical solutions for elliptical finite-conductivity fractures. Paper SPE 22656 presented at the 66th Annual Technical Conference and Exhibition, Dallas, TX, USA, 6–9 Oct 1991

ValkÓ and Economides. 1998. Heavy Crude Production from Shallow Formations: Long Horizontal Wells Versus Horizontal Fractures. SPE-50421.1998. SPE International Conference on Horizontal Well Technology, 1-4 November, Calgary, Alberta, Canada

Vincent, M. C., Pearson, C. M., Kullman, J. 1999. Non-Darcy and multiphase flow in propped fractures: case studies illustrate the dramatic effect on well productivity. Paper SPE-54630 presented at the 1999 SPE Western Regional Meeting held in Anchorage, Alaska, May 26-28.

Wahl, Harry A., Jr. 1956. An Electrolytic Model Study of the Effect of Horizontal Fractures on Well Productivity", MA thesis, The U. of Oklahoma, Norman, Okla

Wang and Jia, 2014. A general productivity model for optimization of multiple fractures with heterogeneous properties. Journal of Natural Gas Science and Engineering. 21 (2014) 608-624

Y. Wei and Economides, 2005. Transverse Hydraulic Fractures From a Horizontal Well. SPE-94671. SPE Annual Technical Conference and Exhibition, 9-12 October, Dallas, Texas

Zeng, F. and Zhao, G. 2010. The Optimal Hydraulic Fracture Geometry Under Non-Darcy Flow Effects. J. Pet. Sci. Eng. 72 (1–2): 143–157.
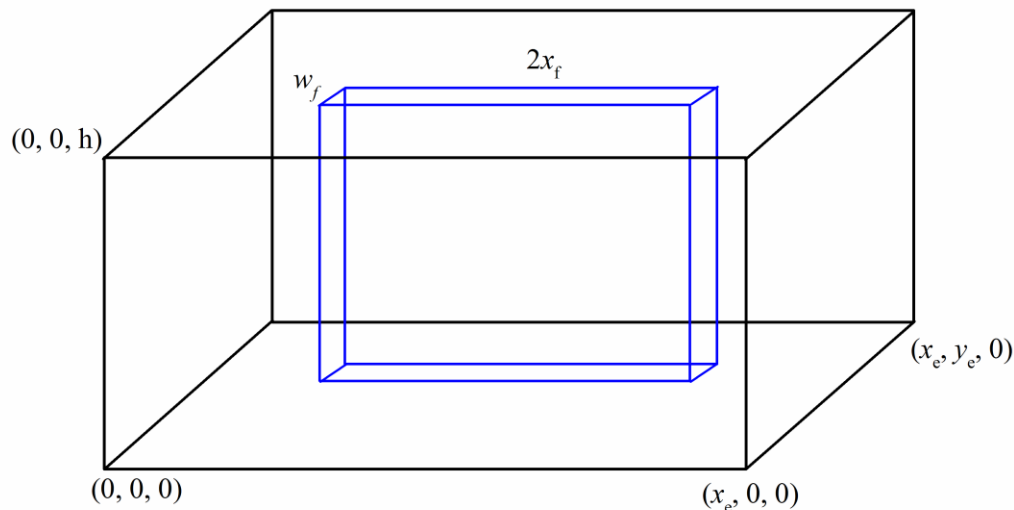
Fig.1 Schematic of a vertical fracture in a rectangular reservoir
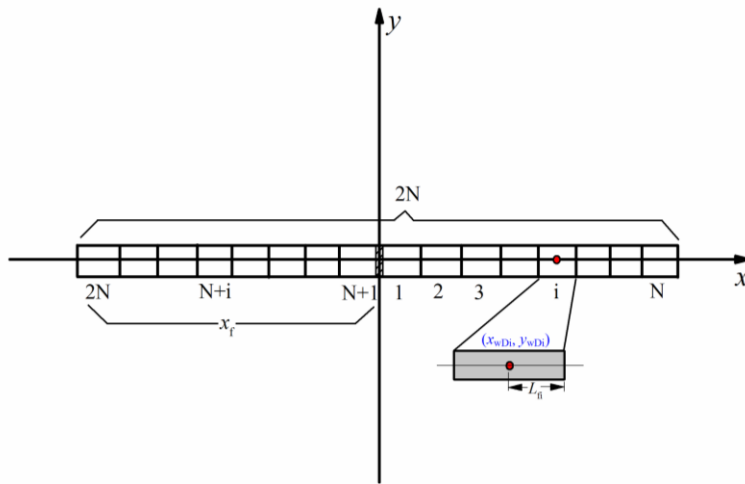
Fig.2 Fracture divided into 2N equal segments
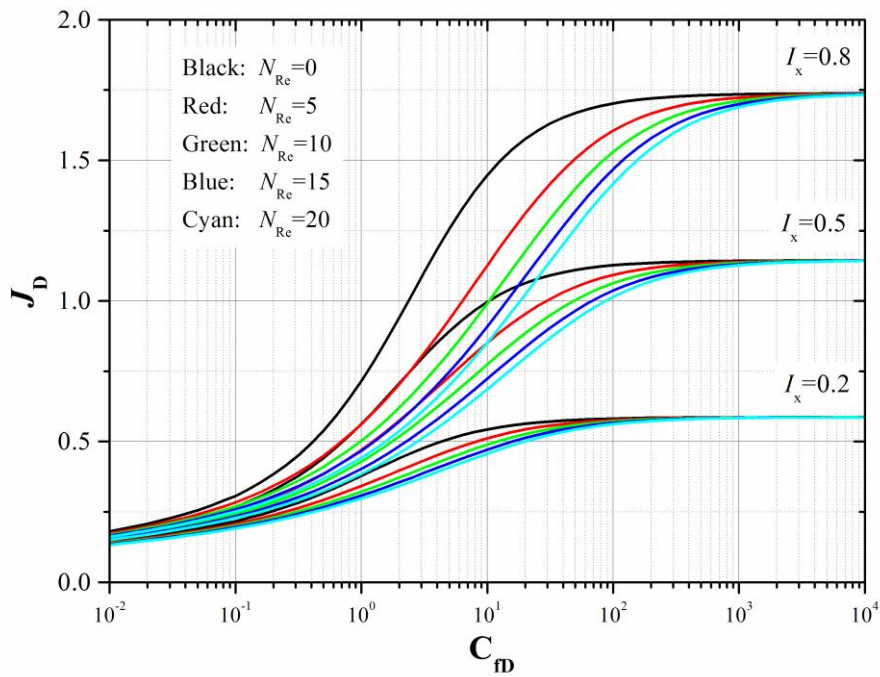
Fig.3 Fracture performance as a function of dimensionless fracture conductivity, penetration ratio and the Reynolds number (square drainage area)
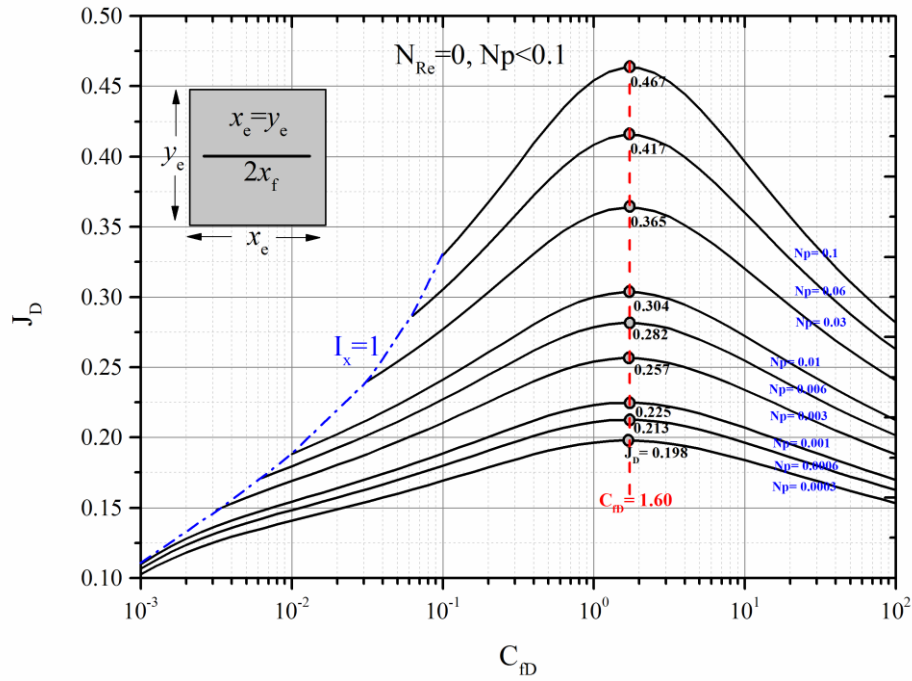
Fig.4 Fracture performance at selected proppant number (N_{Re}=0, Np<0.1) (square drainage area)
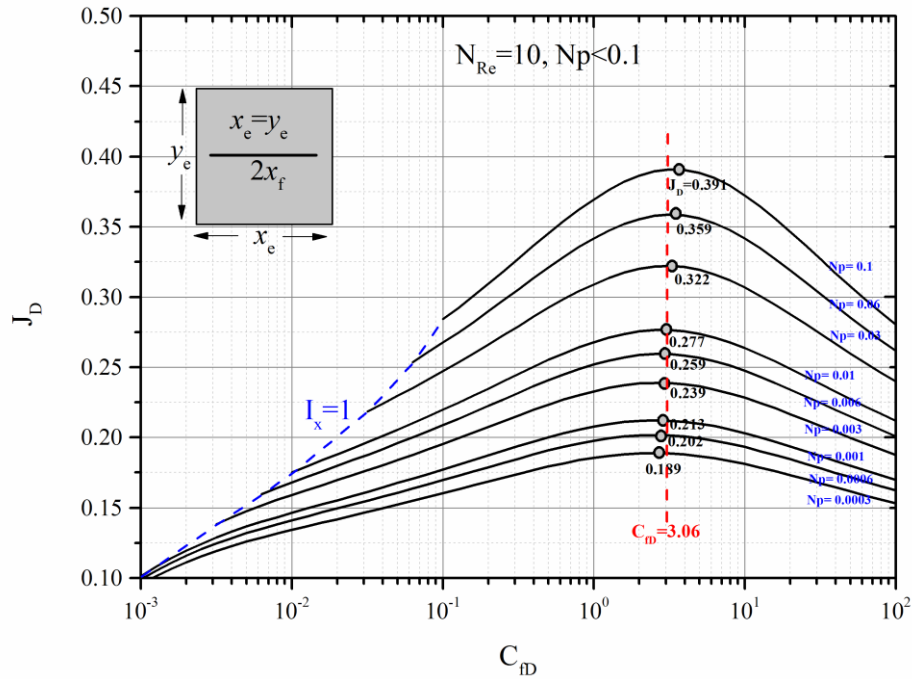
Fig.5 Fracture performance at selected proppant number (N_{Re}=10, Np<0.1, square drainage area)
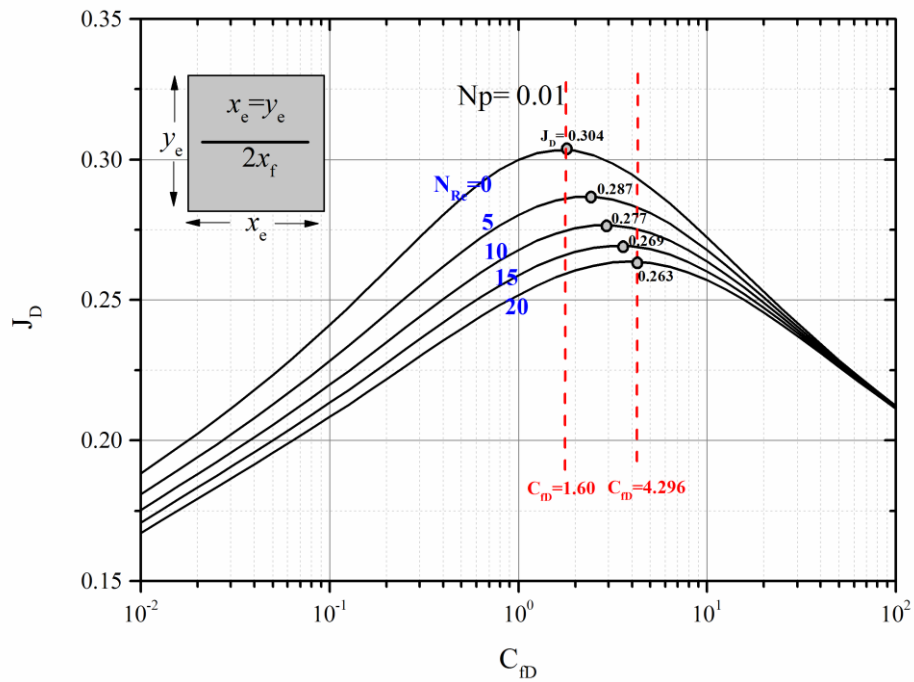
Fig.6 The effect of N_{Re} on the productivity index (Np=0.01) (square drainage area)
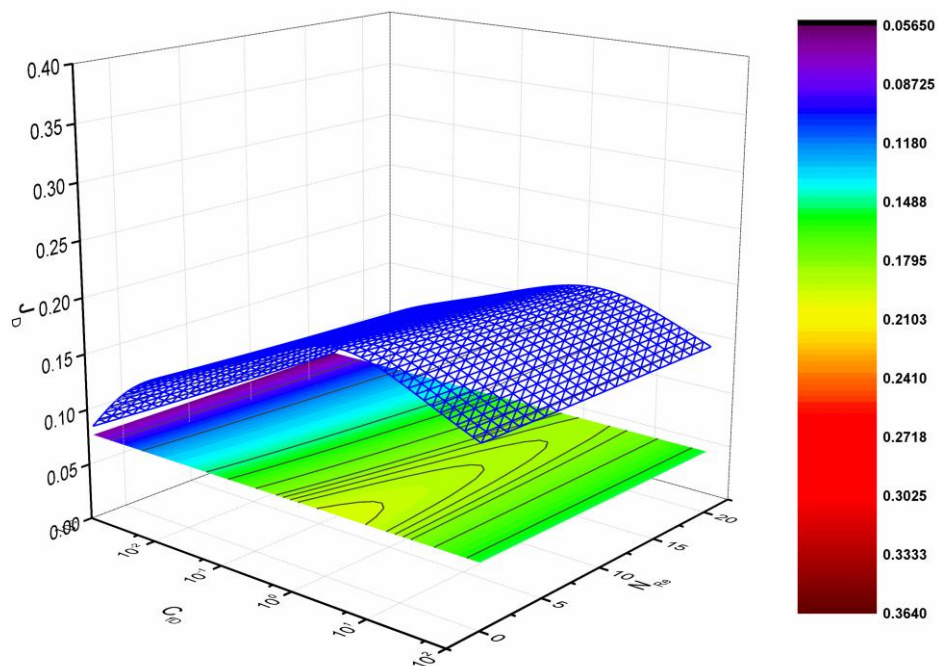
Fig.7 The 3-D color map and its top view of the productivity index, fracture conductivity and the Reynolds number at Np=0.0003 (square drainage area)
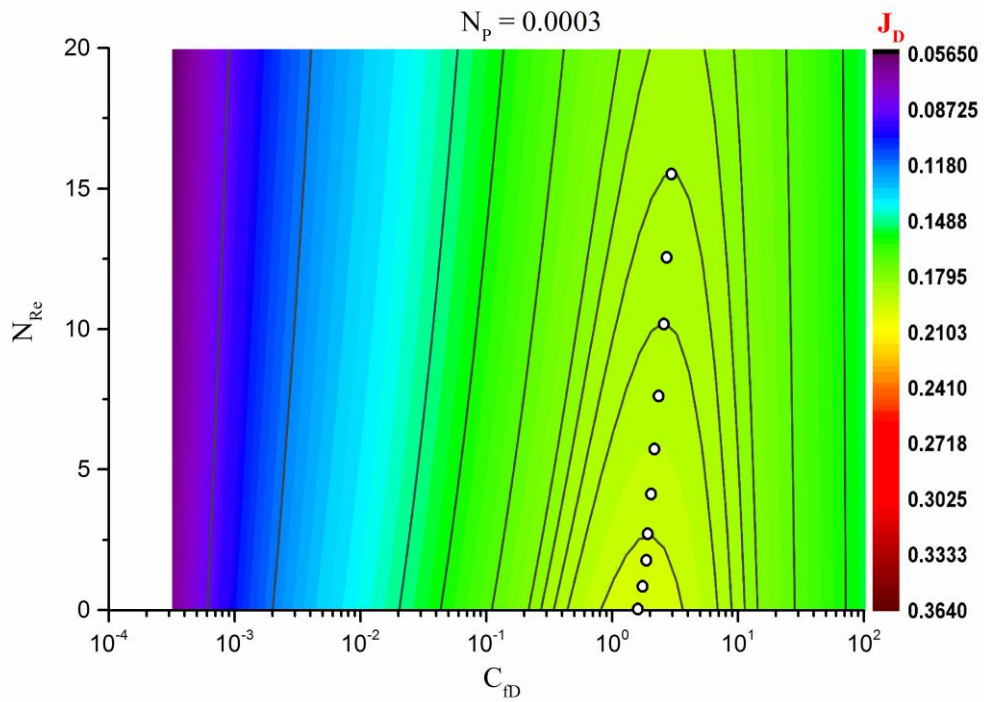
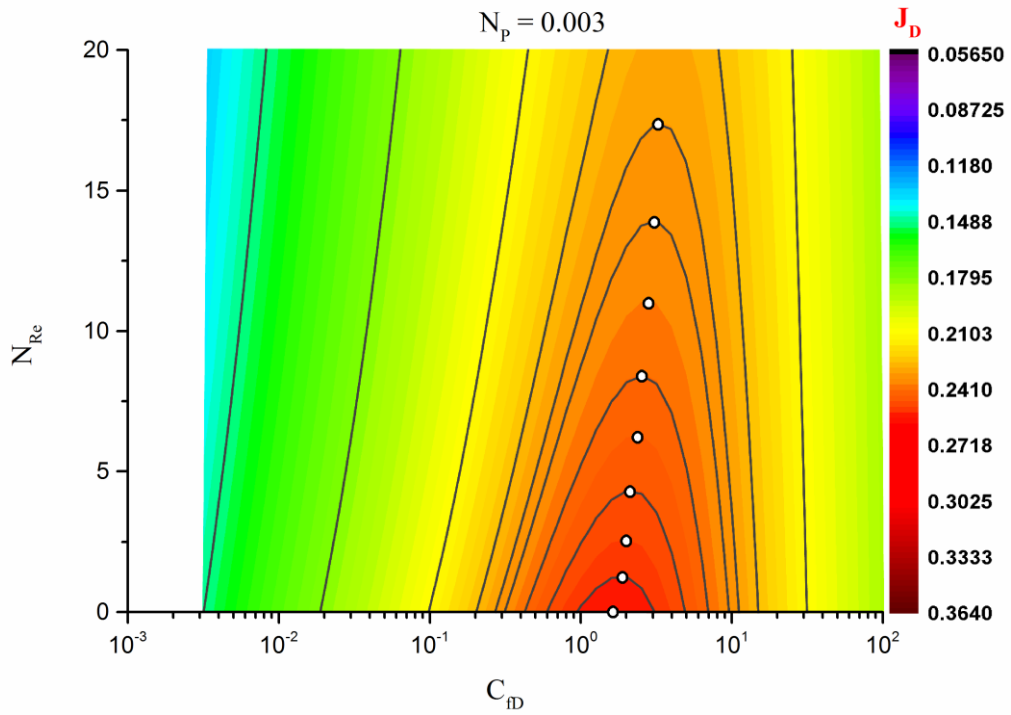Fig.8 The 2-D color map of the productivity index, fracture conductivity and the Reynolds number at Np=0.0003 (square drainage area)
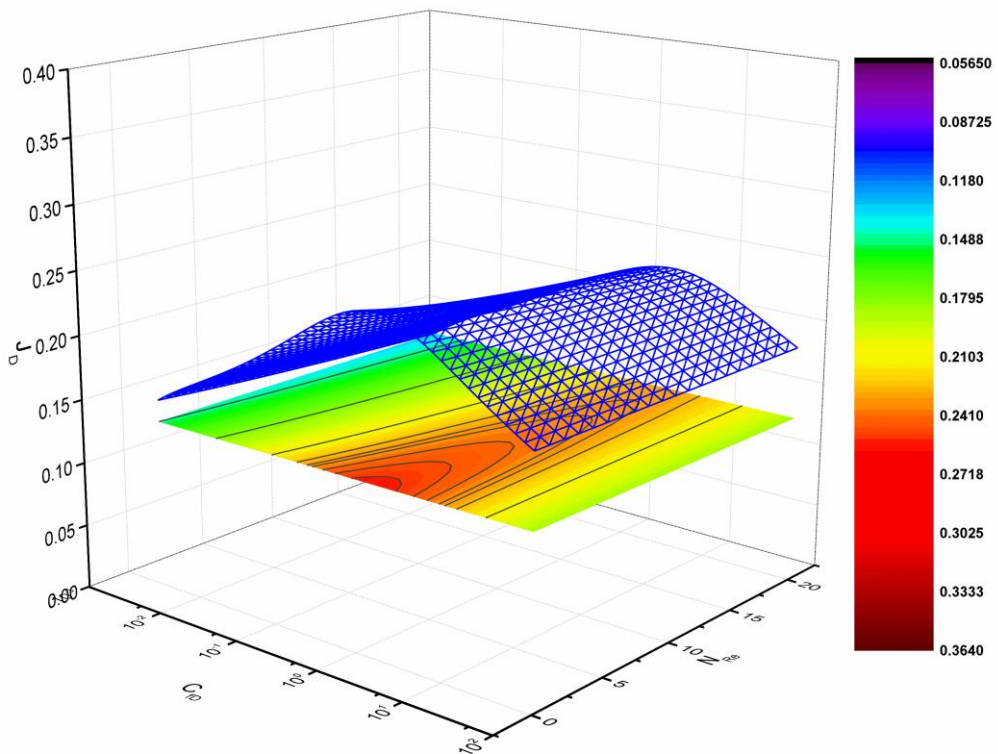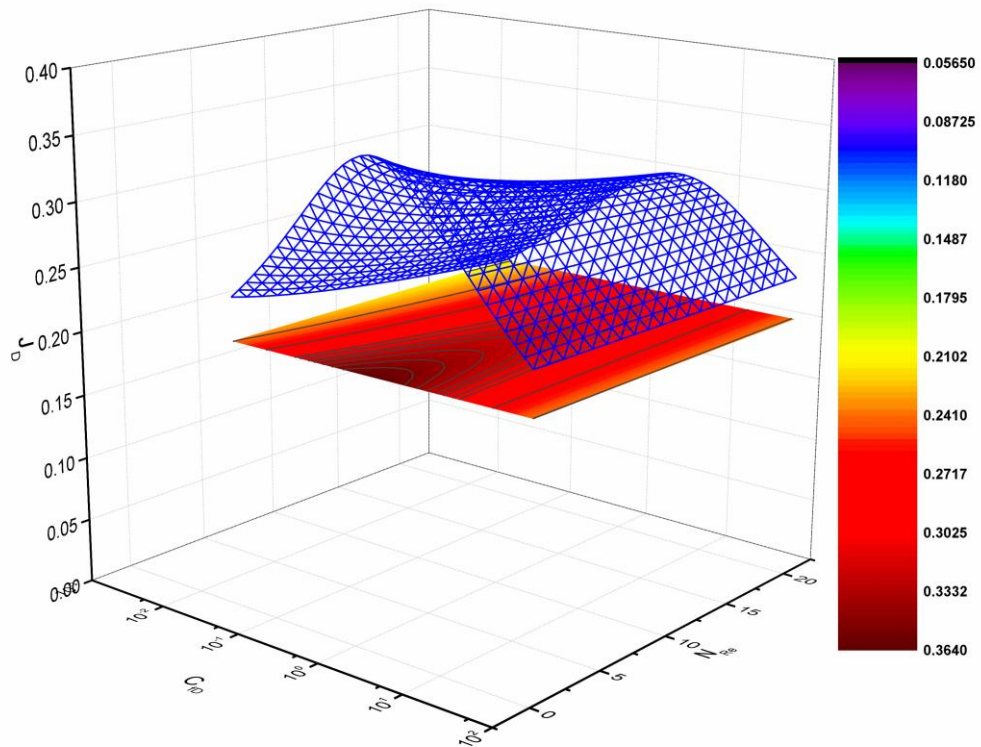

Fig.9 The 3-D color map and its top view of the productivity index, fracture conductivity and the Reynolds number at Np=0.003 (square drainage area)

Fig.10 The 2-D color map of the productivity index, fracture conductivity and the Reynolds number at Np=0.003 (square drainage area)

Fig.11 The 3-D color map and its top view of the productivity index, fracture conductivity and the Reynolds number at Np=0.03 (square drainage area)
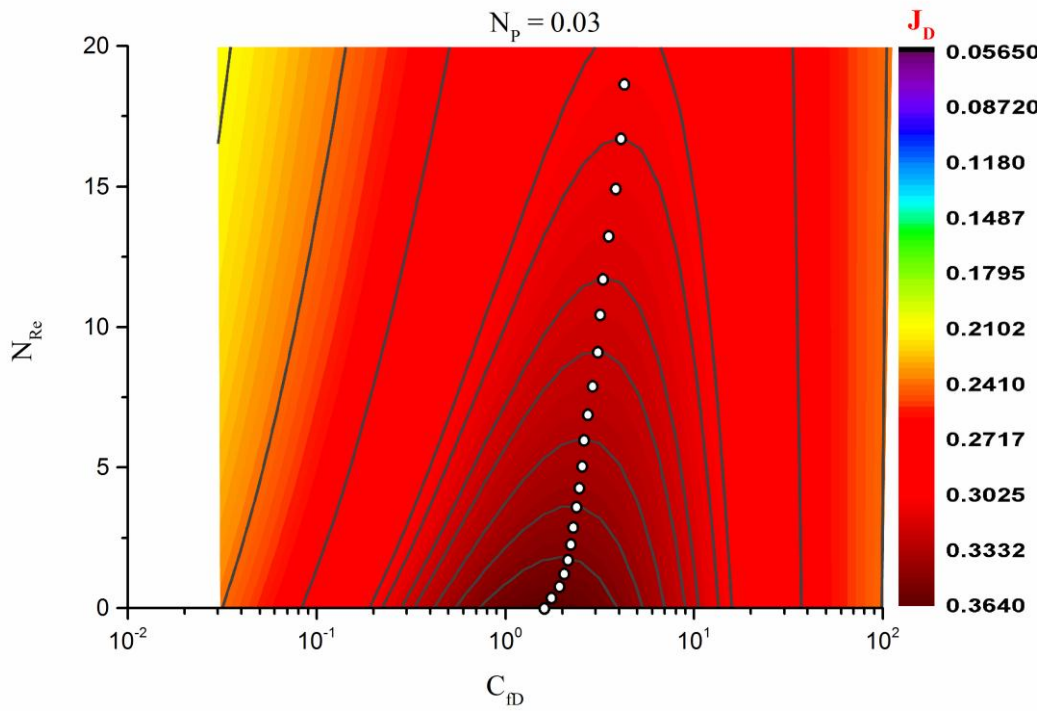
36

Fig.12 The 2-D color map of the productivity index, fracture conductivity and the Reynolds number at Np=0.03 (square drainage area)
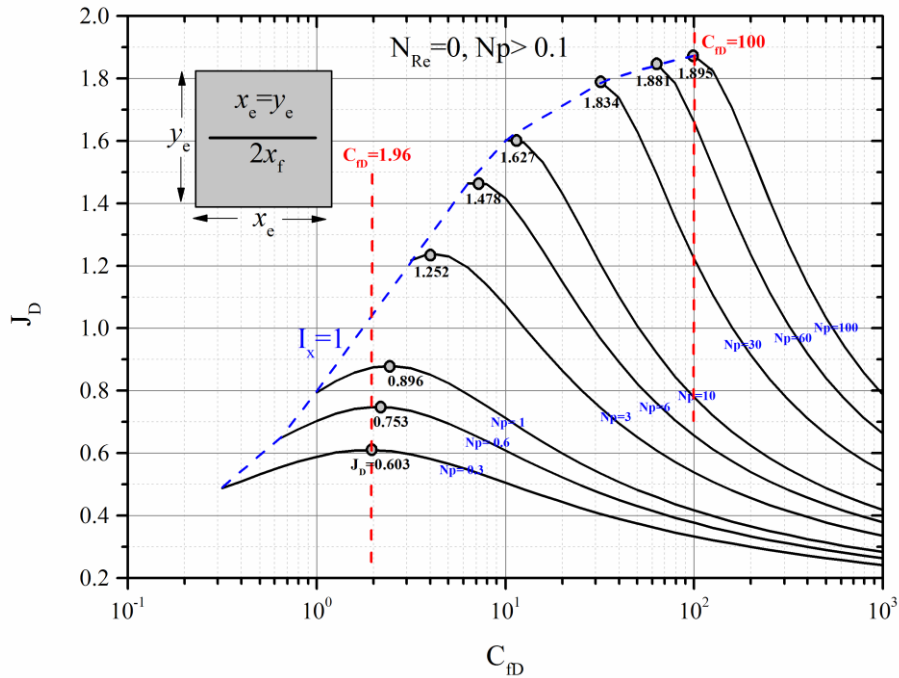

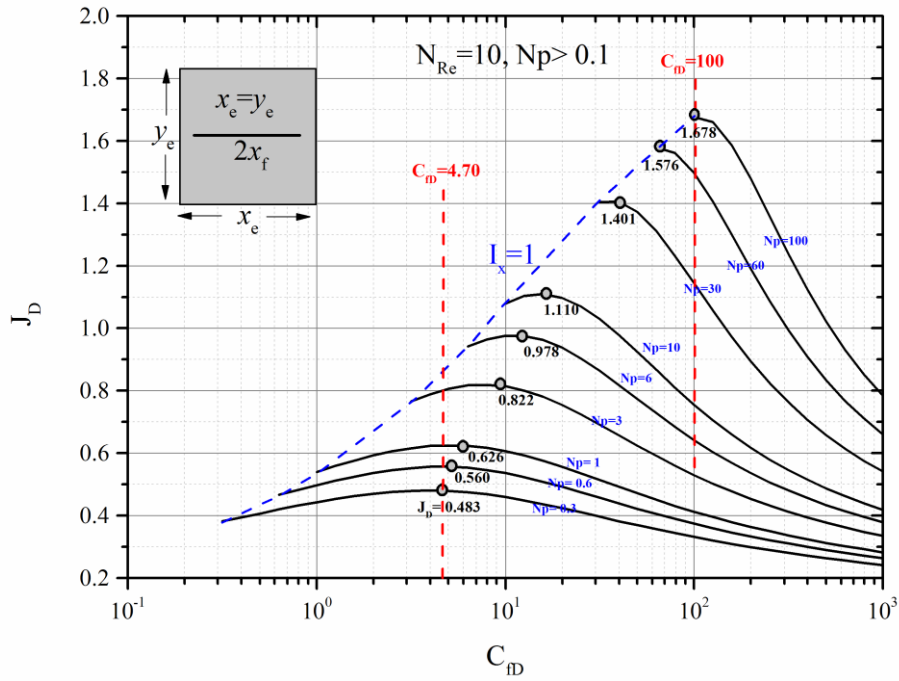Fig.13 Fracture performance at selected proppant number (N_{Re}=0, Np>0.1) (square drainage area)

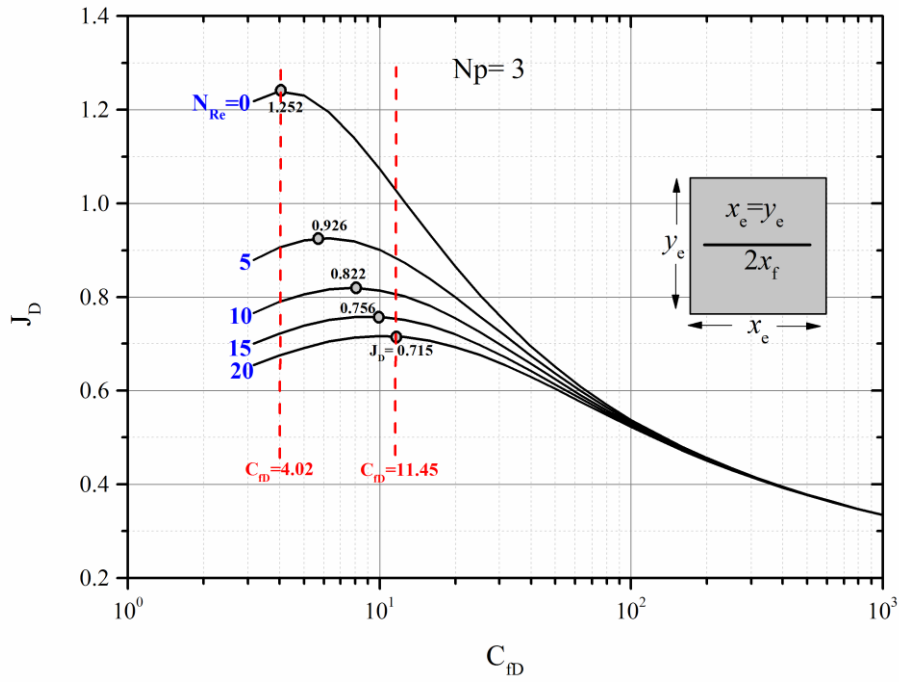Fig.14 Fracture performance at selected proppant number (N_{Re}=10, Np>0.1) (square drainage area)

Fig.15 The effect of N_{Re} on the productivity index (Np=3) (square drainage area)

Fig.16 The 3-D color map and its top view of the productivity index, fracture conductivity and the Reynolds number at Np=0.3 (square drainage area)

Fig.17 The 2-D color map of the productivity index, fracture conductivity and the Reynolds number at Np=0.3 (square drainage area)
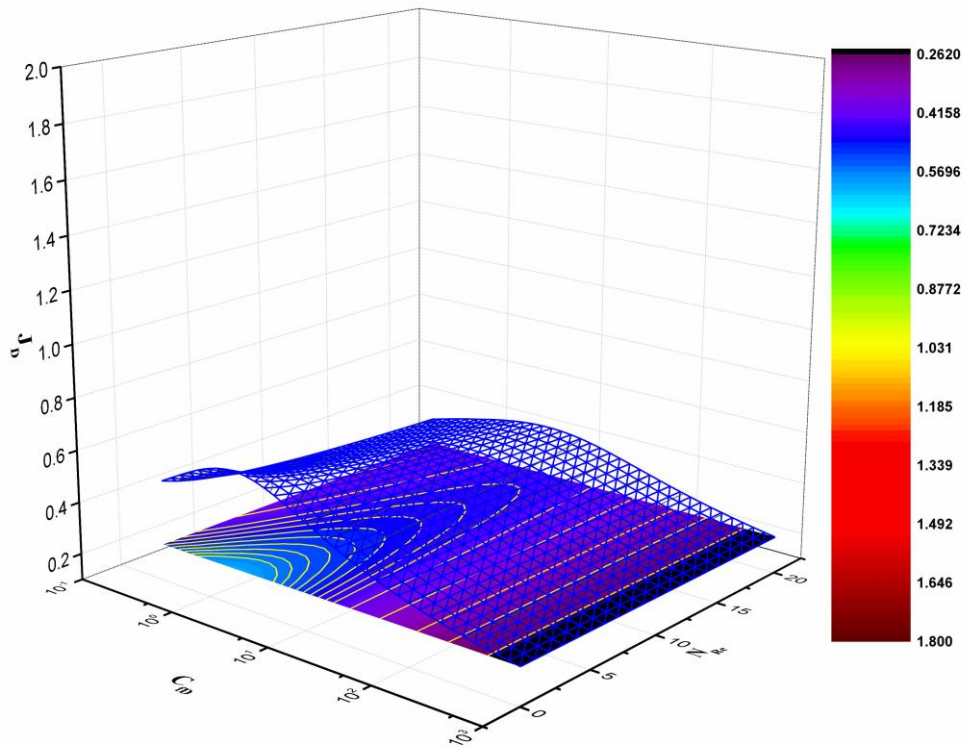
Fig.18 The 3-D color map and its top view of the productivity index, fracture conductivity and the Reynolds number at Np=3 (square drainage area)

Fig.19 The 2-D color map of the productivity index, fracture conductivity and the Reynolds number at Np=3 (square drainage area)

40

Fig.20 The 3-D color map and its top view of the productivity index, fracture conductivity and the Reynolds number at Np=30 (square drainage area)
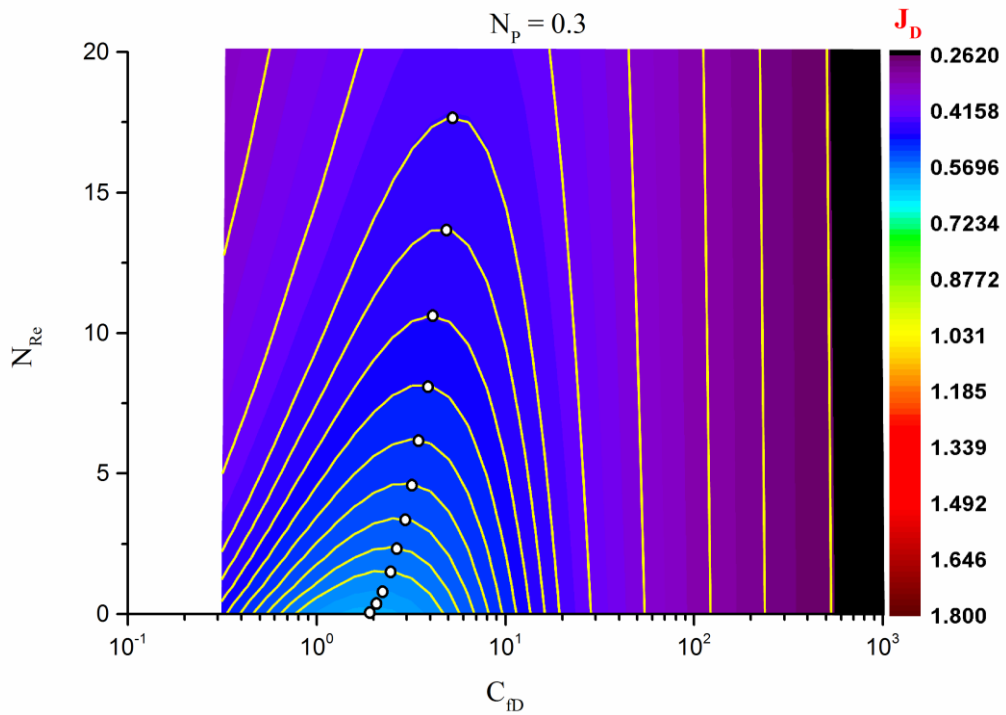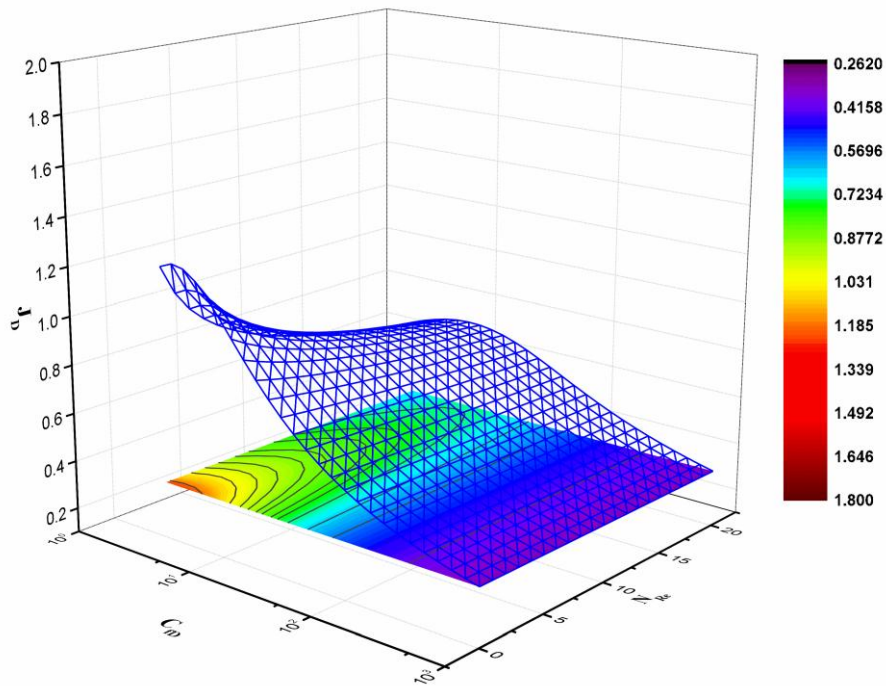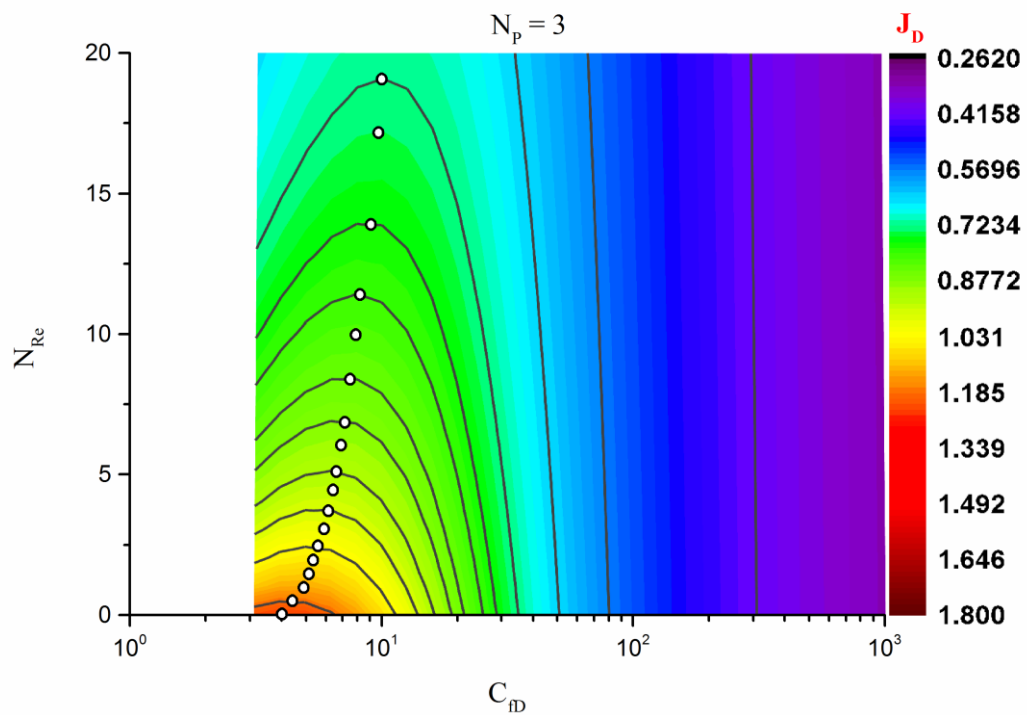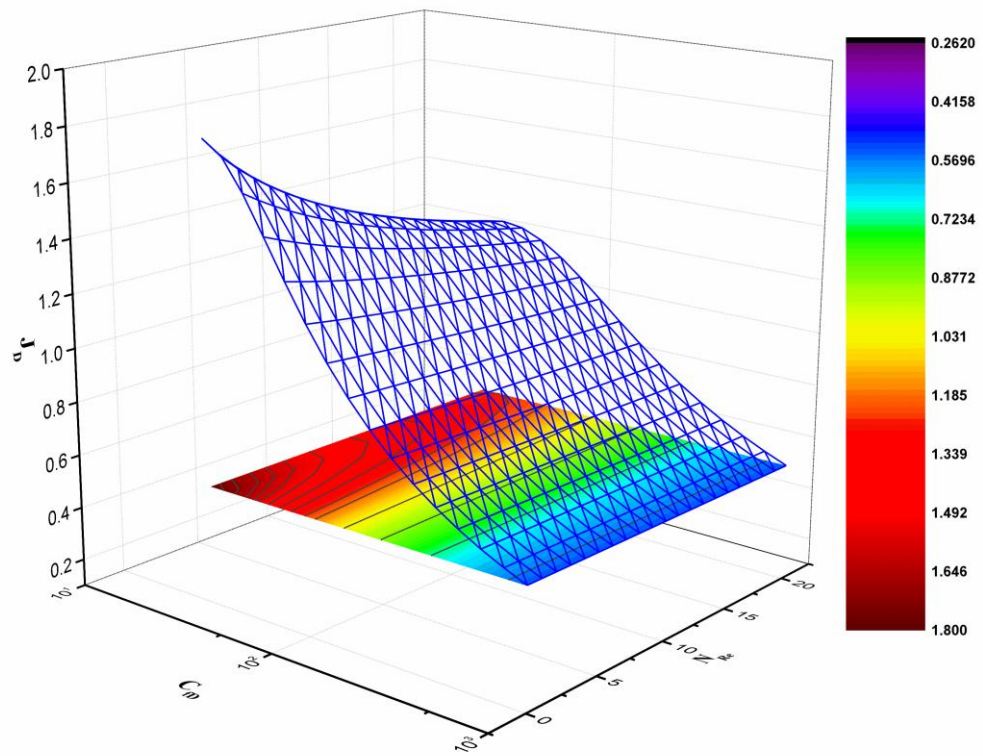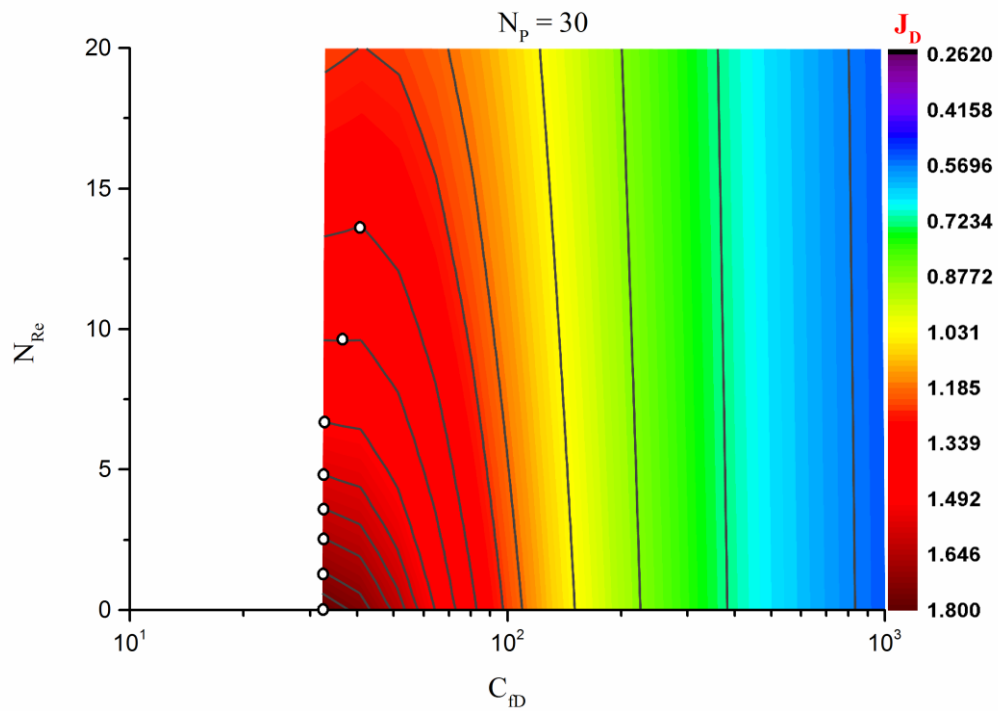

Fig.21 The 2-D color map of the productivity index, fracture conductivity and the Reynolds number at Np=30 (square drainage area)

Fig.22 contents:

Black line: $N_{Re} = 0$
Red line: $N_p = 3.383$

$(N_p = 3.383, N_{Re} = 0)$

This paper		Lopez et al. (2004)	
N_{Re}	N_p	Equivalent N_{Re}	Equivalent N_p
0	3.383	0	3.383
2	3.383	0	1.128
4	3.383	0	0.676
6	3.383	0	0.483
8	3.383	0	0.376
10	3.383	0	0.308
12	3.383	0	0.26
14	3.383	0	0.226
16	3.383	0	0.199
18	3.383	0	0.178
20	3.383	0	0.161
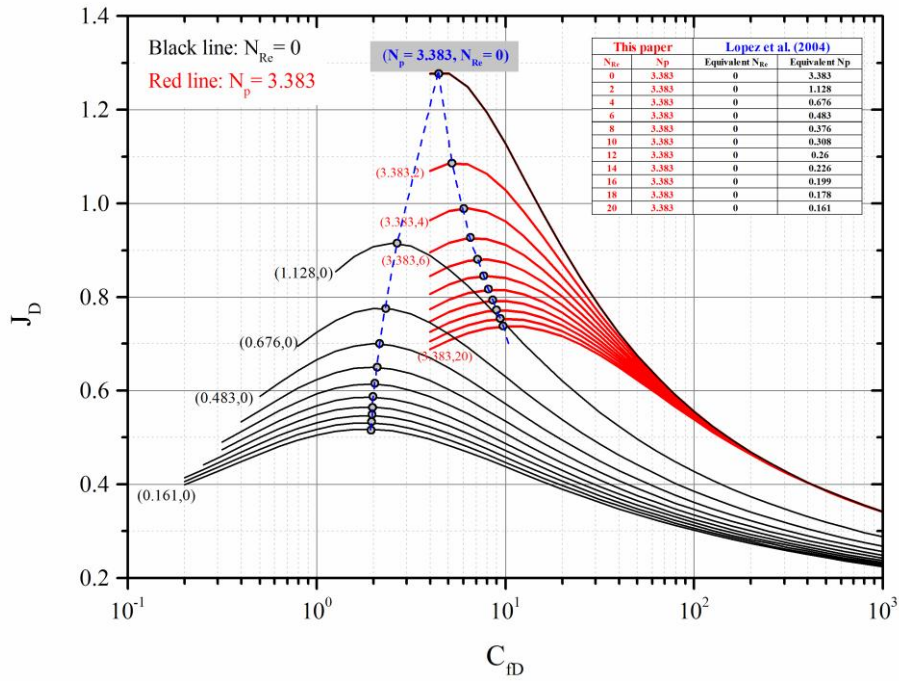
Fig.22 Comparisons of the productivity index with Lopez et al. method

$Np = 3.383$，$N_{Re} = 16.5$

(9.942,0.7655)

Fig.23 The optimization of the fracture conductivity with Np=3.383 and N_{Re}=16.5 (square drainage area)

Table 1 Comparison between ValkÓ-Economides result and our work (xeD/yeD=1)

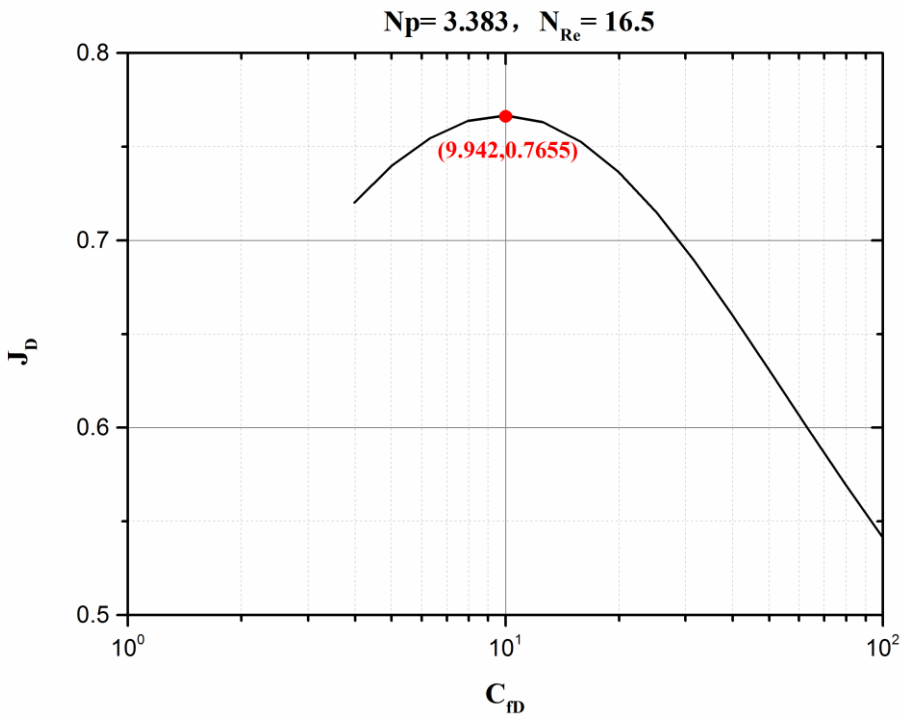| C_{fD}	Ix=0.1			Ix=0.3			Ix=0.6			Ix=1.0		
	ValkÓ-Economides (1998)	This paper	Error	ValkÓ-Economides (1998)	This paper	Error	ValkÓ-Economides (1998)	This paper	Error	ValkÓ-Economides (1998)	This paper	Error
			%			%			%			%
0.01	0.1428	0.1297	11.6815	0.1727	0.1531	11.3550	0.2026	0.1717	15.2658	0.2193	0.1882	14.1476
0.1	0.1927	0.1878	2.0339	0.2469	0.2365	4.2121	0.2977	0.2820	5.2872	0.3544	0.3266	7.8382
1	0.2986	0.2999	0.5058	0.4436	0.4439	0.0631	0.6197	0.6169	0.4422	0.8096	0.7944	1.8824
10	0.3861	0.3964	0.5517	0.6829	0.6880	0.7527	1.1499	1.1570	0.6209	1.6042	1.6033	0.0605
100	0.4162	0.4166	0.2282	0.7489	0.7502	0.1656	1.3232	1.3305	0.5570	1.8785	1.8726	0.3151
1000	0.4171	0.4188	0.4651	0.7546	0.7574	0.3737	1.3415	1.3519	0.7745	1.9127	1.9061	0.3451
Average			2.5777			2.8204			3.8246			4.0981

Table 2 Basic parameters for calculation of the productivity index (Henry D. Lopez-Hernandez et al., 2004)

Basic model parameters	values	Basic model parameters	values
Drainage radius, r_e, ft	745	Viscosity of gas, μ, mPa.s	0.0205
Fracture height, h_f, ft	139	Gas compressibility factor, z	0.944
Reservoir thickness, h, ft	39	Injected proppant mass, M_{p-2w}, lbm	60000
Reservoir permeability, k, md	0.2	Proppant specific gravity, SGp	2.62
Fracture permeability, k_f, md	134248	Gas specific gravity, SGg	0.644
Reservoir porosity, ϕ, %	10	Molecular weight of air, Mair , lb/lb mole	29
Fracture porosity, ϕ_p, %	40	Coefficient of Beta factor, a	3.7E11
Reservoir temperature, T_{res}, °R	680	Coefficient of Beta factor, b	1.35
Reservoir pressure, p_{res}, psi	5254	Coefficient of Beta factor, c	0
Bottom pressure, p_{wf}, psi	1400		

Table 3 Comparisons of the optimal fracture conductivity and maximum productivity index with Henry D. Lopez-Hernandez et al. method

	This paper			Henry D. Lopez-Hernandez et al. (2004)				Error,%	
N_{Re}	N_p	C_{fDopt}	J_{Dopt}	Equivalent N_{Re}	Equivalent N_p	C_{fDopt}	J_{Dopt}	C_{fDopt}	J_{Dopt}
0	3.38	4.44	1.279	0	3.38	4.44	1.279	0	0
2	3.38	5.25	1.086	0	1.128	2.67	0.915	49.14	15.75
4	3.38	5.96	0.987	0	0.676	2.31	0.775	61.24	21.48
6	3.38	6.47	0.927	0	0.483	2.16	0.701	66.62	24.38
8	3.38	7.09	0.88	0	0.376	2.08	0.65	70.66	26.14
10	3.38	7.65	0.843	0	0.308	2.04	0.616	73.33	26.93
12	3.38	8.24	0.815	0	0.26	1.99	0.587	75.85	27.98
14	3.38	8.63	0.79	0	0.226	1.98	0.565	77.06	28.48
16	3.38	9.03	0.771	0	0.199	1.95	0.547	78.41	29.05
18	3.38	9.41	0.753	0	0.178	1.94	0.531	79.38	29.48
20	3.38	9.86	0.735	0	0.161	1.93	0.517	80.43	29.66

Table 4 Basic parameters and the results for the fracture optimization

Parameters	kg	k_f	$k_{f\text{-}eff}$	N_p	N_{Re}	C_{fDopt}	J_{Dopt}	x_f	w_f
Units	md	md	md					ft	ft
This paper	0.2	134248	-	3.383	16.5	9.942	0.7655	385.113	0.0057
Henry D. Lopez-Hernandez et al. (2004)	0.2	134248	12407	0.31	9.82	1.75	0.63	278	0.00786

Appendix A: Unit Conversion Factors

SI Metric Conversion Factors

bbl $\times$ 0.1589874 m^3

cP $\times$ 0.001   Pa s

ft $\times$ 0.3048   m

ft$^2 \times$0.0929	m^2
psi$\times$6.894757	kPa

Highlights:

(1) Propose a semi-analytical solution of the pseudosteady-state (PSS) productivity index under the non-Darcy flow condition in a rectangular reservoir

(2) Reveal the effect of the Reynolds number, the proppant number and the fracture conductivity on the dimensionless productivity index

(3) Discuss the adaptability of the Darcy-flow UFD (Unified Fracture Design) curves under the non-Darcy flow condition

(4) Develop a new model for optimization of the fracture parameters